Metal oxide thin film-based low-temperature-operating solid oxide fuel cell by interface structure control

15

J.-W. Son[*,†]
[*]Korea Institute of Science and Technology (KIST), Seoul, Republic of Korea,
[†]Korea University of Science and Technology, Daejeon, Republic of Korea

15.1 What is solid oxide fuel cell (SOFC)?

A fuel cell is an electrochemical device that converts the chemical energy of the fuel oxidation reaction directly into electrical energy. This process involves the ion movements through an electrolyte placed between electrodes, the oxidation of fuel at an anode (fuel electrode), and the reduction of the oxidant at a cathode (air electrode). A cell composed of an anode, an electrolyte, and a cathode is called a unit cell. A solid oxide fuel cell (SOFC) is a fuel cell the electrolyte and electrodes of which are mainly based on solid oxide, that is, metal oxide materials.

In most of the cases, oxygen ions (O^{2-}) are the main charge carriers so oxygen ion conducting oxides are essential materials for SOFCs. The ionic conductivity of the metal oxide materials can be induced by doping of the cation with a difference valence. For example, a Y^{3+} ion substitution of a Zr^{4+} ion in ZrO_2 generates oxygen vacancies to keep the charge balance, and this induces the oxygen ion conduction (Y_2O_3-doped ZrO_2 or yttria-stabilized zirconia, YSZ, $Zr_{1-x}Y_xO_{2-x/2}$). Doped ZrO_2 and doped CeO_2 such as gadolinia-doped ceria (Gd_2O_3-doped CeO_2, GDC, $Ce_{1-x}Gd_xO_{2-x/2}$) are most representative electrolyte materials for SOFCs.

Some special metal oxides possess proton (hydrogen ion, H^+) conducting capability and these can be the base materials for the proton-conducting SOFC, or protonic ceramic fuel cells (PCFC). Doped $BaZrO_3$ and doped $BaCeO_3$ are most representative electrolyte materials for PCFCs. In Fig. 15.1, the structure and basic operating principles of SOFC and PCFC are shown. As gas-phase oxidant and fuel are supplied, the electrodes have a gas-permeable (porous) structure. The electrolyte has a gas-impermeable (dense) structure to separate oxidant and fuel and electrochemical reactions at both electrodes, not to directly combust the fuel.

There are various methods to categorize the types of the SOFC. For example, if the shape of the unit cell is used to classify SOFC cells, there are tubular, planar, flat-tubular SOFCs, and so on. A unit cell of the SOFC can be categorized by the component which is in charge of the structural support of the whole cell as well. If the electrolyte is thick and supports the whole structure, then the SOFC cell is called

Metal Oxide-Based Thin Film Structures. https://doi.org/10.1016/B978-0-12-811166-6.00015-7

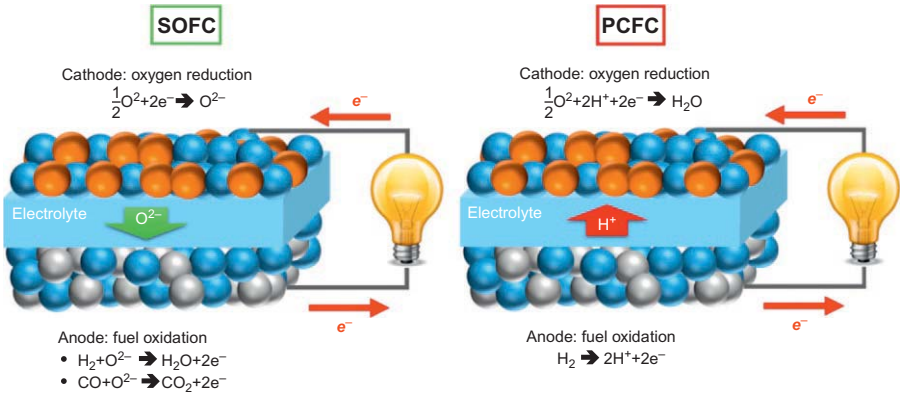

Fig. 15.1 Components and basic reactions of metal oxide-based fuel cells: solid oxide fuel cell (SOFC) and protonic ceramic fuel cell (PCFC).

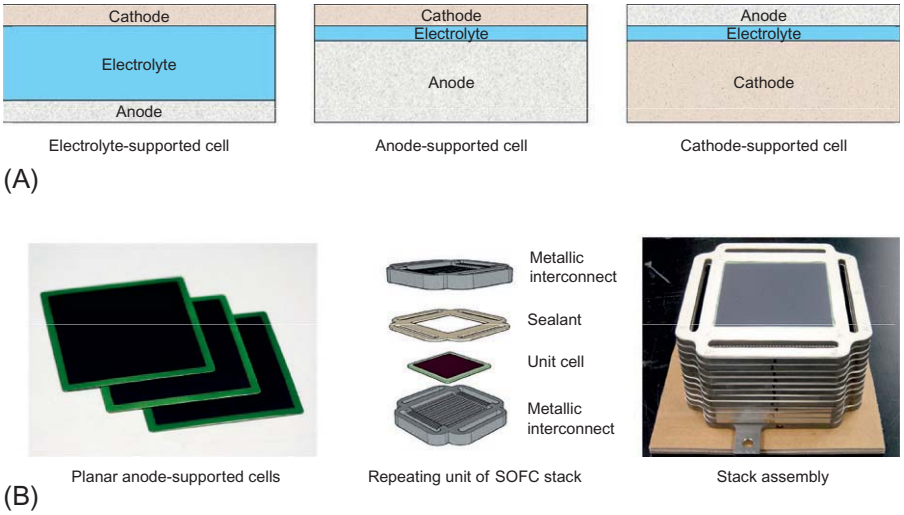

Fig. 15.2 (A) SOFC unit cell types categorized by the supporting component. (B) Unit cells and stack of planar-type anode-supported SOFC fabricated at Korea Institute of Science and Technology (KIST).

as an electrolyte-supported cell. If the electrode is thick and supports the whole structure, then the SOFC cell is named as an electrode-supported cell. The unit cells are serially connected to increase the operating voltage and the capacity of the power generation, and this connected unit is called a stack [1]. In Fig. 15.2, the configurations of the cells by the supporting component and examples based on a planar type anode-supported SOFC are presented.

Among various fuel cell types, an SOFC operates at the highest temperature range. It generally operates at temperatures higher than 700°C. Due to this high-temperature operation, the SOFC exhibits high efficiency, high specific power, and power

density [2]. A unique and significant advantage of the SOFC is that it can be operated with fuels other than pure hydrogen, as can be seen in the anode reaction involving carbon monoxide indicated in Fig. 15.1. This is because hydrocarbon fuels break up easily into H_2 and CO, and the carbon deposition can be less serious at high temperatures. Owing to this fuel flexibility, SOFC can be used on currently existing hydrocarbon fuel infrastructures [2–4].

15.2 Why low-temperature-operating SOFC (LT-SOFC) is interesting?

Ironically, the high-temperature operation of SOFCs (HT-SOFCs) limits the commercial development of the technology despite that it is the origin of the above-mentioned merits. The high operating temperatures require expensive refractory materials in the system components, hampering the cost-competitiveness of the technology. It also causes fast degradation due to the chemical reactions and physical defects generated at the interfaces. These issues slow down the utilization of the SOFC technology for large-scale power generation in the commercial sector. In addition, quick start-up and shutdown are not possible; and the weight and volume of the thermal insulation are substantial in HT-SOFCs. These restrict the application of the technology to the transportation and portable power sources in spite of the fuel flexibility.

In this regard, there have been intensive research efforts to lower the operating temperature of the SOFC. If the operating temperature can be lowered, then inexpensive materials can be used. For example, cheap stainless steels can be used instead of expensive refractory metals like Inconel for the interconnect that occupies a substantial volume and cost of the planar SOFC stack [5,6]. At lower temperatures, the detrimental chemical reaction and physical agglomeration of the cell components can be suppressed. Low-temperature operation significantly reduces the burden of the thermal insulation and enable quick start-up and shutdown, which expands the category of application to smaller and mobile power sources.

In general, HT-SOFCs are fabricated by using ceramic processing, including raw powder packing, forming and shaping, and high-temperature sintering. However, in realizing LT-SOFCs, significant differences in terms of structures and/or materials are required in comparison with those of HT-SOFCs. Especially when the structures of the SOFC are modified to make it operable at low temperatures, metal oxide thin films are considered to play a critical role; therefore, this chapter addresses the application of metal oxide thin films on LT-SOFCs especially in terms of the interface structure control.

15.3 Operating temperature range of LT-SOFC

Before discussing further details of the LT-SOFC, the operating temperature range for the SOFC should be categorized. How low temperature is low in the SOFC? In this chapter, the low-temperature regime is defined to be $\leq$650°C, following the definitions in Refs. [2,4]. This temperature range may be called as intermediate

temperature (IT) range, especially when other fuel cell types such as polymer electrolyte membrane fuel cells (PEMFC) generally operating at $T \leq 100°C$ are considered together. For example, the Reliable Electricity Based on Electrochemical Systems (REBELS) project funded by Advanced Research Projects Agency-Energy (ARPA-E), the US Department of Energy (DOE), defines fuel cells operating at 200–500°C as IT-fuel cells (ITFCs) [7].

Nevertheless, in the SOFC, nonconventional structures and materials of the cell components are required to be operated at $T \leq 650°C$ [4]. In terms of the electrolyte, for example, ultrathin electrolytes or electrolytes made of highly conductive novel materials are required. Therefore, the operating temperatures range of LT-SOFCs will be considered as $T \leq 650°C$ hereafter. The high temperature and intermediate temperature SOFCs, which are fabricated by the conventional ceramic processing and operate at $T > 650°C$ are categorized as the HT-SOFC in this chapter as a counterpart of the LT-SOFCs.

15.4 Approaches for lowering the operating temperature of SOFCs

The prerequisite of realizing LT-SOFCs is not to compromise the cell performance while reducing the operating temperature. As the ionic conduction at the electrolyte and the catalytic reaction at the electrode are thermally activated processes, the resistance related to these reactions increase exponentially as the temperature decreases. For instance, conductivity and resulting resistance of the ionic conduction is expressed by the equation below [8]:

$$\sigma T = \sigma_o e^{-\frac{E_a}{kT}} \tag{15.1}$$

$$\begin{aligned} \text{Area Specific Resistance (ASR)} &= \text{Area} \times \text{Resistance} \\ &= \frac{\text{Length}\,(L)}{\sigma} \\ &= \frac{LT}{\sigma_o} e^{\frac{E_a}{kT}} \end{aligned} \tag{15.2}$$

where E_a is an activation energy of the ionic conduction. Therefore, if only the operating temperature is lowered for an HT-SOFC, then the power output would decrease to an unacceptable level.

Here is an example. A conventional planar anode-supported SOFC the components of which are composed of the most common SOFC materials: a nickel and YSZ composite anode; a YSZ electrolyte; a GDC buffer; and a lanthanum strontium manganite ($La_{1-x}Sr_xMnO_{3-\delta}$, LSM) and YSZ composite cathode, can produce 0.77 W/cm^2 at the cell voltage of 0.7 V at 800°C. The power density, however, plummets to 0.287 W/cm^2 at 0.7 V when the operating temperature is lowered to 650°C [9].

There can be two main approaches to mitigate the performance reduction at low operating temperatures. One is to use novel materials with superior properties to those of the conventional materials, such as electrolyte materials with high ionic conductivity and electrode materials with exquisite catalytic activity [10]. In this approach,

generally, sintering-engaged conventional ceramic processing is the main fabrication method. Highly performing electrolyte materials such as doped ceria, doped bismuth oxide, and novel electrode materials such as double perovskite-structure cathode materials are used [2,4]. Some reported extraordinarily high performance such as peak power density reaching ~2 W/cm^2, even near 3 W/cm^2 at 650°C [11,12].

The main advantage of this approach is that ceramic processing, which is rather cheap and familiar to commercial production is used. However, the novel materials used in this approach is not widely accepted in the major SOFC field due to the stability, price, availability, synthesizability, etc. In addition, this approach has little relation to the metal oxide thin film because the structural dimensions of the cell components using novel materials are not different from those of the conventional HT-SOFCs. Therefore, although this has high potential and is actively researched, it will not be extensively discussed in this chapter.

The other approach is to reduce the resistance increase accompanying lowering the operating temperature by changing the structural dimensions of the cell component, not by changing the material. Thinning down the electrolyte would reduce the ohmic resistance originating from the electrolyte. If an YSZ electrolyte has thickness of around 1.5 μm, then it has a similar resistance value at 500°C to that of a 15 μm-thick YSZ electrolyte at 700°C [3]. If the particle size of the electrodes can be reduced to nm ~ sub-μm scale, then the electrode reaction site density can increase dramatically, so the polarization resistance at lower temperature can be effectively reduced, both at the cathode and the anode [13–17]. These are the main reasons why the technologies for the metal oxide thin films such as thin film deposition and microfabrications, which can create the thin electrolyte and nanostructure electrodes, have drawn significant attention during the past decade.

In this approach, widely accepted and proven SOFC materials are used, so one can be less concerned about the uncertainty of the materials. The most commonly considered disadvantage of the approach is the expensiveness of the fabrication method as it usually involves expensive vacuum deposition apparatus and sophisticated processing technologies. However, it is often ignored that the high reliability and production yield of the thin film technology can significantly reduce the fabrication defects related to the high-temperature processing of the multilayered SOFC. This can effectively reduce huge waste of the materials and components originating from the processing defects. In addition, the performance increase owing to the utilization of the thin film deposition may effectively reduce the number of cells and thus that of the repeating unit in the stack for generating a required power output, which results in the significant cost down of the stack [6]. In this regard, proper application of metal oxide thin films can provide substantial contribution to this field of research, both technically and economically.

15.5 Challenges in realizing proper metal oxide thin film structure in LT-SOFCs

The primary interest of the interface-related issues in metal oxide thin films, which is also treated intensively in other chapters of this book, is regarding formation, characterization, and application based on the peculiar properties originated from the

epitaxial relationship at the interface. Nevertheless, in LT-SOFC devices, although there are intensive efforts to utilize the remarkable properties of the epitaxial metal oxide thin films to the LT-SOFC, it is hard to take advantages of these properties in reality.

The epitaxial interface of metal oxide thin films is generally parallel to the substrate surface. The remarkable properties such as gigantic ionic conduction increase in SOFC electrolyte materials, therefore, usually appears along the interface of the multilayer epitaxial films [18–21]. In a real SOFC, the ionic movement direction is perpendicular to the interface, not parallel, as shown in Fig. 15.1. In addition, one of main reasons for this property is considered to be the strain induced at the interfaces, which can be relaxed at the elevated temperature of SOFC operation. Therefore, it is not highly possible to fully utilize the phenomenon in working SOFCs. There exist some special cases that may exploit the interface phenomenon in metal oxide thin films: like a coplanar single chamber SOFC that utilizes in-plane conduction at the electrolyte by placing both anode and cathode at the same surface of the electrolyte [22,23]; and vertically aligned nanostructures (VAN) of which interfaces are along the ionic conduction paths of SOFCs [24,25]. However, due to certain restrictions in terms of the operating and/or fabrication conditions, these cases are not commonly used in working SOFC devices yet.

The main challenge of using metal oxide thin films in SOFCs is rather macroscale in comparison with the sophisticated epitaxial films. It is about how to realize gas-impermeable, thin, and dense metal oxide films for the electrolyte; how to realize nanoporous and sufficiently thick films for the electrode; and how to secure the interfacial integrity between totally different microstructures and materials of the layers, that is, the dense electrolyte and the porous electrodes, which can sustain at elevated temperatures. The first and the most important and the biggest challenge would be obtaining a proper electrolyte structure, because it is the most basic requirement to realize the operating SOFC. In fact, the hurdle to achieve the dense electrolyte by metal oxide thin film deposition in the SOFC configuration is not trivial, and only handful of approaches are successful in realizing the desirable structure.

When depositing thin films, substrates are required and the film structure is dependent on the condition of the surface of the substrate. In general, electrolyte materials have higher resistivity than electrode materials, thus for lowering the operating temperature, an electrode-supported SOFC configuration as described in Figs. 15.2 and 15.3 is preferred to avoid a high ohmic resistance originating from a thick electrolyte. The electrode should have a porous structure because the gas-phase reactants, fuel and oxidant, must transport for the fuel cell operation. Therefore, a gas-impermeable, dense electrolyte should be fabricated over a porous electrode for the electrode-supported SOFC.

Nevertheless, it is extremely challenging to deposit a dense thin film over a porous substrate because it contains plenty of discontinuity, which appears like deep steps and significant roughness. If a highly directional physical vapor deposition (PVD) such as evaporation, sputtering, and pulsed laser deposition (PLD) is used, one possibility is that the film stacks up without covering the sidewall of the pore, as shown in Fig. 15.4A. More realistic situation is that directionality of the deposit is scattered

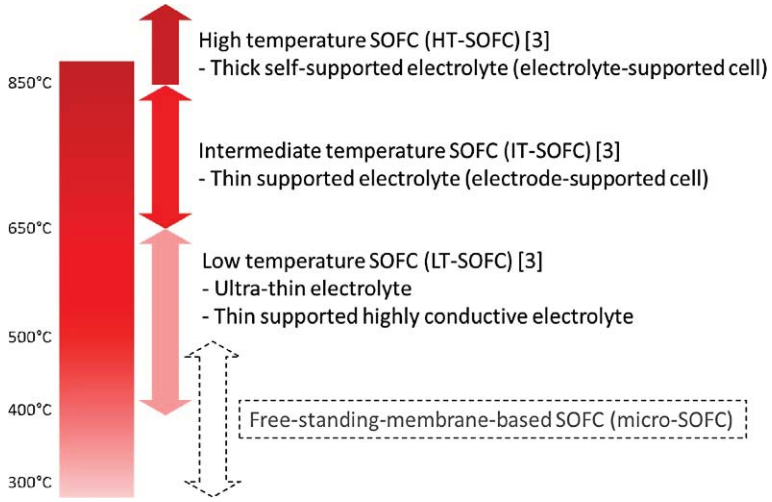

Fig. 15.3 Categories of SOFC based on the operating temperatures [4]. Usual operating temperature range of free-standing-membrane-based SOFC (micro-SOFC), which will be treated as an LT-SOFC type in this chapter, is indicated together.

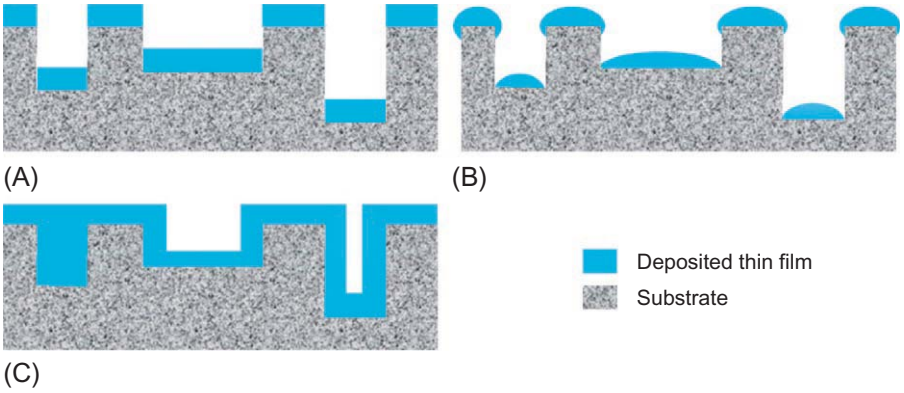

Fig. 15.4 Schematics showing thin film morphologies deposited over porous substrate surfaces. (A) and (B) are when a deposition method such as PVD is used—(A) highly directional and (B) realistic. (C) is when a conformal deposition method such as CVD is used.

to a certain extend while it travels toward the substrate and the nucleation of the thin film would occur at the surface of the substrate and the rim of the pore, as shown in Fig. 15.4B. For Fig. 15.4A and B, when the pore size is big and the film is thin, it is impossible to achieve a continuous, dense structure of the thin film. However, when a conformal deposition such as a chemical vapor deposition (CVD) is used, all surfaces and sidewalls of the substrate may be covered, so pore clogging can happen when a continuous film structure is obtained, as shown in Fig. 15.4C.

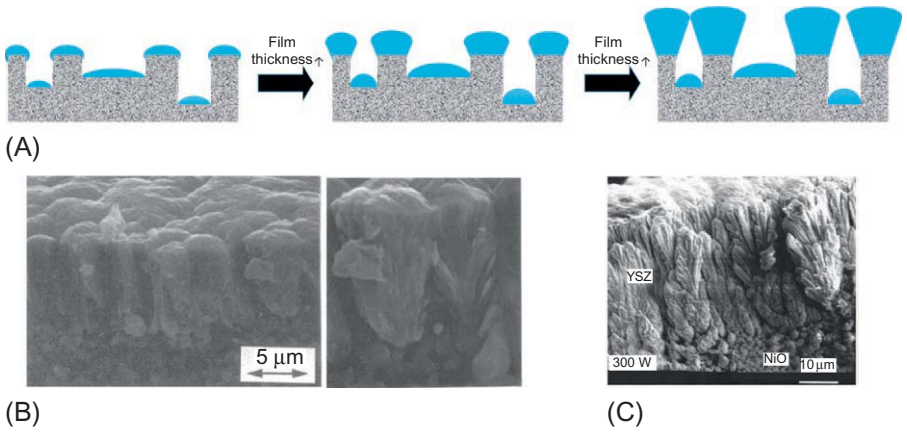

Fig. 15.5 (A) Schematics representation showing thin film morphology change when thickness increases, (B) YSZ electrolyte deposited over porous cathode [26], and (C) deposited over porous anode [27].
Reproduced with permission from T. Tsai, S.A. Barnett, J. Electrochem. Soc 142 (1995) 3084–3087, Copyright (1995) The Electrochemical Society, and from A. Nagata, H. Okayama, Vacuum 66 (2002) 523–529, Copyright (2002) Elsevier.

What happens if the thickness of the thin film increases to cover the pores? If thin film is being deposited as in the case of Fig. 15.4B, the film deposited on the top surface and the pore rim grow. When the diameter of the deposited domain grows large enough, then the domain can touch each other to cover the pore, as described in Fig. 15.5A. The film structure consisting of domains appear as inverted cones, as shown in Fig. 15.5B and C.

There have been certain trials to deposit sufficiently thick electrolyte films over porous supports to fabricate SOFCs [26–29]. This approach is unsuccessful mainly due to two reasons. Although sufficiently thick films reaching 10 µm are deposited, it was not successful to obtain theoretical open-circuit voltage (OCV) [26–29]. The OCV is a cell voltage at zero current, and in an ideal condition, it is determined by the oxygen potential difference across the electrolyte, that is, difference at the cathode–electrolyte and the anode-electrolyte interfaces. Therefore, if the electrolyte is a perfect ionic conductor and has no gas leakage, then the OCV should reach the theoretical value. Low OCVs indicate that there is gas leakage and/or the electrolyte has ion-electron mixed conduction. As a perfect ionic conductor, YSZ, was used as the electrolyte material, the low OCV values obtained from the above cases imply that the pinholes penetrating the entire thickness of the electrolyte exist at the points where the film domains contact. These pinholes drop the cell voltage, therefore the cell performance would drop in accordance. Moreover, the pinholes are where the fuel and oxidant mix and direct combustion of fuel can happen, which eventually result in the catastrophic destruction from the electrolyte membrane to the unit cell and stack.

The second reason is that there is no reason to use thin film deposition to obtain this thick electrolyte. It is time-consuming and expensive than other coating methods

based on ceramic processing such as screen printing to fabricate 10 μm thick electrolyte, especially considering that an SOFC with a deposited electrolyte yielded inferior cell performance to that with a screen-printed electrolyte [29]. With this thickness, it is nonsense to say thin film deposition is used for reducing the ohmic resistance of the electrolyte.

Therefore, direct deposition of the electrolyte thin film over the porous electrodes is not a proper method to obtain gas-impermeable, thin, and dense electrolytes for LT-SOFCs. This indicates that the conventional configuration of the SOFC cannot be used for realizing LT-SOFCs based on metal oxide thin films. From the following section, it will be addressed how this issue can be resolved.

15.6 Free-standing-membrane-based LT-SOFCs: Micro-SOFCs

The most straightforward method to obtain a thin and dense electrolyte is to deposit the thin electrolyte over a dense and flat surface of the substrate. How can one obtain porous electrode structure at the bottom of the electrolyte in this case?

In 2007, an extreme case of the ultrathin electrolyte-supported SOFC design using microelectromechanical systems (MEMS) technology was invented by researchers at Stanford University [30]. The core idea is to deposit the electrolyte over a dense surface to obtain a thin and dense electrolyte structure, expose the bottom of the electrolyte, and then deposit porous electrode later. In Fig. 15.6A, the process flow used in Ref. [30] is described.

1. A silicon nitride layer, which is an etch mask deposited by CVD over a silicon substrate.
2. An ultrathin YSZ electrolyte was deposited over the top surface of the silicon nitride layer.
3. The silicon nitride layer is patterned at the bottom side of the substrate to open a window for the chemical etching of the substrate before the electrolyte deposition.
4. The whole structure was dipped in a KOH solution to remove the substrate existing underneath the silicon nitride and the electrolyte.
5. The silicon nitride layer was removed by the reactive ion etching (RIE) to expose the bottom surface of the electrolyte.
6. The porous platinum was deposited on top and bottom surfaces of the electrolyte to form electrodes.

Ultrathin, free-standing electrolyte-membrane-supported SOFCs can be fabricated by the above process. As microfabrication including MEMS is used extensively for this cell type, these are typically called micro-SOFCs. It is possible that the chemical etching (step 4) is performed prior to the electrolyte deposition (step 2) to form a silicon nitride free-standing membrane first [31]. The electrolyte film is deposited over the silicon nitride membrane later. This variation of the process flow is described in Fig. 15.6B. In either case, the electrolyte is deposited over a dense surface to secure the dense microstructure.

Ever since the first successful report of the micro-SOFC [30], extensive research efforts were put in this field for about a decade. To increase the active area of the

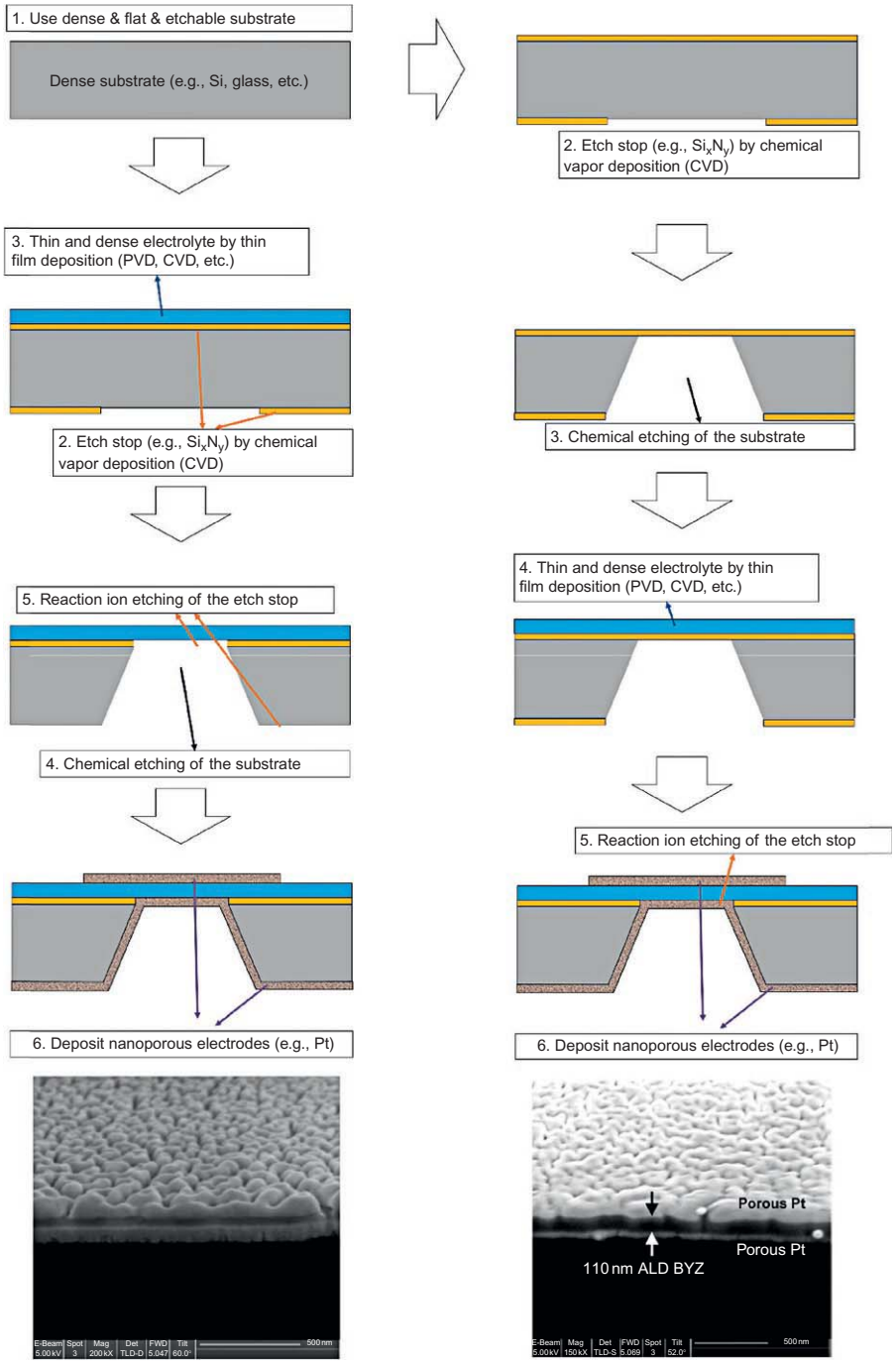
1. Use dense & flat & etchable substrate
Dense substrate (e.g., Si, glass, etc.)
3. Thin and dense electrolyte by thin film deposition (PVD, CVD, etc.)
2. Etch stop (e.g., Si_xN_y) by chemical vapor deposition (CVD)
5. Reaction ion etching of the etch stop
4. Chemical etching of the substrate
6. Deposit nanoporous electrodes (e.g., Pt)
2. Etch stop (e.g., Si_xN_y) by chemical vapor deposition (CVD)
3. Chemical etching of the substrate
4. Thin and dense electrolyte by thin film deposition (PVD, CVD, etc.)
5. Reaction ion etching of the etch stop
6. Deposit nanoporous electrodes (e.g., Pt)
Porous Pt
Porous Pt
110 nm ALD BYZ
(A)
(B)

membrane, three-dimensional structures such as corrugated or crater-like patterned membranes were developed, as shown in Fig. 15.7 [32–35]. Remarkable low-temperature performance reaching a peak power density of 1.3 W/cm^2 at 450°C was reported [34]. Substrates other than Si wafers like patternable glass were tried as well [36]. To overcome one of the most critical shortcomings of the micro-SOFC, the extremely small cell area, scale-up of the membrane using supporting grid patterns were investigated [37–39]. In Ref. [39], exhaustive collection of the properties of the micro-SOFC reported up to date is presented.

In several variations of the micro-SOFC, it has been attempted to deposit or form the porous bottom electrode first, then the electrolyte was deposited over the porous layer [36,40]. In these cases, appropriate OCV values were not obtained. The main reason is that fully gas-impermeable electrolyte thin film could not be obtained due to the porous deposition surface condition, as was described in the previous section. The dependency of the microstructure of the electrolyte on the deposition surface is systematically analyzed in Ref. [40]. In Fig. 15.8, the microstructure of the YSZ electrolyte deposited on the flat silicon nitride surface, the nanoporous surface with pore diameter ~40 nm, and the nanoporous surface with pore diameter ~60 nm are compared. The YSZ films were deposited in the same deposition conditions; therefore, the difference in the microstructure is sorely affected by the deposition surface. In contrary to the dense electrolyte structure obtained over the dense and flat surface shown in Fig. 15.8A, it can be clearly observed that the inverted cone-shaped grains resulted from the nucleation and growth over the porous surface in Fig. 15.8B and C, and the resulting voids can penetrate up to substantial thickness of the electrolyte, depending on the pore size of the substrate.

This structural difference from the film-substrate interface results in the electrochemical property of the micro-SOFC directly. In Fig. 15.9, the OCV values from various micro-SOFCs based on different deposition surfaces of the electrolyte are compared [40]. The cell fabricated following the process flow of Fig. 15.6 exhibited high OCV (self-supported cell I), whereas a micro-SOFC the electrolyte of which was deposited over porous Pt bottom electrode yielded significantly lower OCVs (self-supported cell II). The AAO-supported cells yielded even lower OCVs. The OCV increase as a function of the YSZ thickness implies that the voids close as the thickness of the electrolyte increases. However, an OCV reaching that of the self-supported cell I could not be reached even with 900-nm-thick electrolytes.

Fig. 15.6, Cont'd Process flow of a micro-SOFC when (A) the back-side etching is performed after the electrolyte deposition, and a resulting SOFC structure [30], and (B) the back-side etching is performed before the electrolyte deposition, and a resulting PCFC structure [31]. The actual cell structures are reproduced with permission from H. Huang, M. Nakamura, P.C. Su, R. Fasching, Y. Saito, F.B. Prinz, J. Electrochem. Soc. 154 (2007) B20–B24, Copyright (2007) The Electrochemical Society, and from J.H. Shim, J.S. Park, J. An, T.M. Gür, S. Kang, F.B. Prinz, Chem. Mater. 21 (2009) 3290–3296, Copyright (2009) American Chemical Society, respectively.

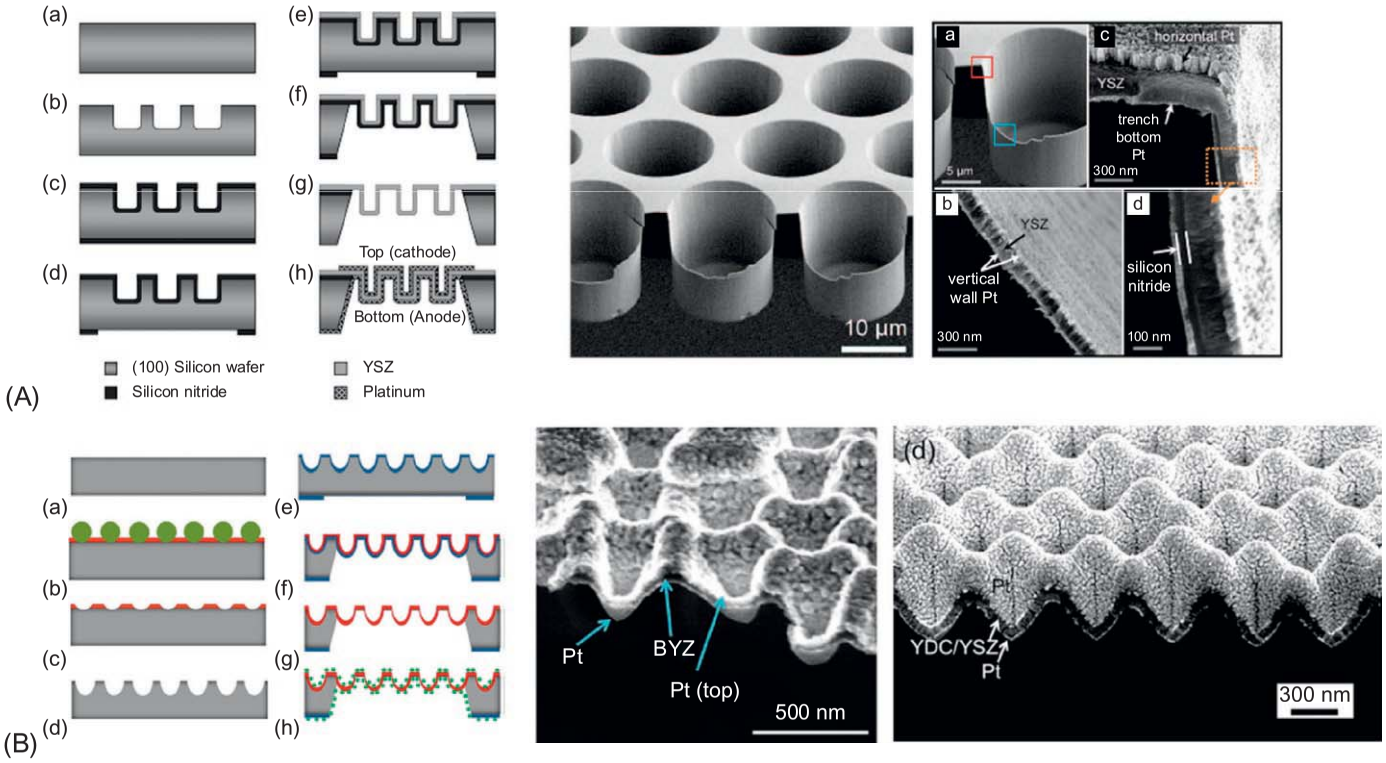

Fig. 15.7 Variations of the micro-SOFC with a 3-D membrane structure: (A) cup-shape corrugated [32] and (B) crater-like structure [33,34]. Reproduced with permission from P.C. Su, C.C. Chao, J.H. Shim, R. Fasching, F.B. Prinz, Nano Lett. 8 (2008) 2289–2292 and J. An, Y.-B. Kim, J. Park, T.M. Gür, F.B. Prinz, Nano Lett. 13 (2013) 4551–4555, Copyright (2008) and (2013) American Chemical Society, and from Y.B. Kim, T.M. Gür, S. Kang, H.-J. Jung, R. Sinclair, F.B. Prinz, Electrochem. Commun. 13 (2011) 403–406, Copyright (2011) Elsevier.

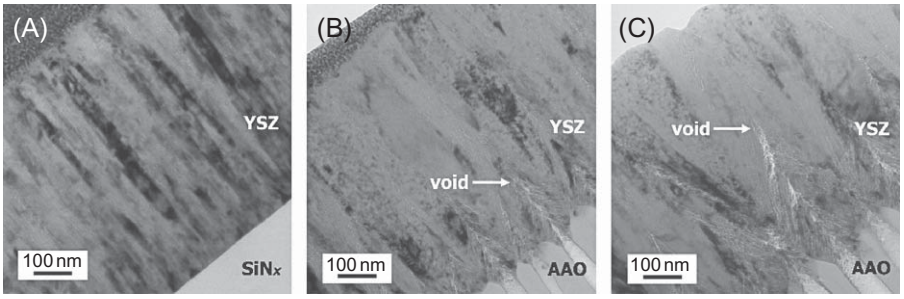

Fig. 15.8 Transmission electron microscopy (TEM) cross-sectional images of 600-nm-thick YSZ films deposited by PLD on a flat silicon nitride substrate (A), and on a porous anodized aluminum oxide (AAO) substrate with 40 nm (B) and 60 nm (C) pores [40].
Reproduced with permission from C.-W. Kwon, J.-W. Son, J.-H. Lee, H.-M. Kim, H.-W. Lee, K.-B. Kim, Adv. Funct. Mater. 21 (2011) 1154–1159, Copyright (2011) John Wiley and Sons.

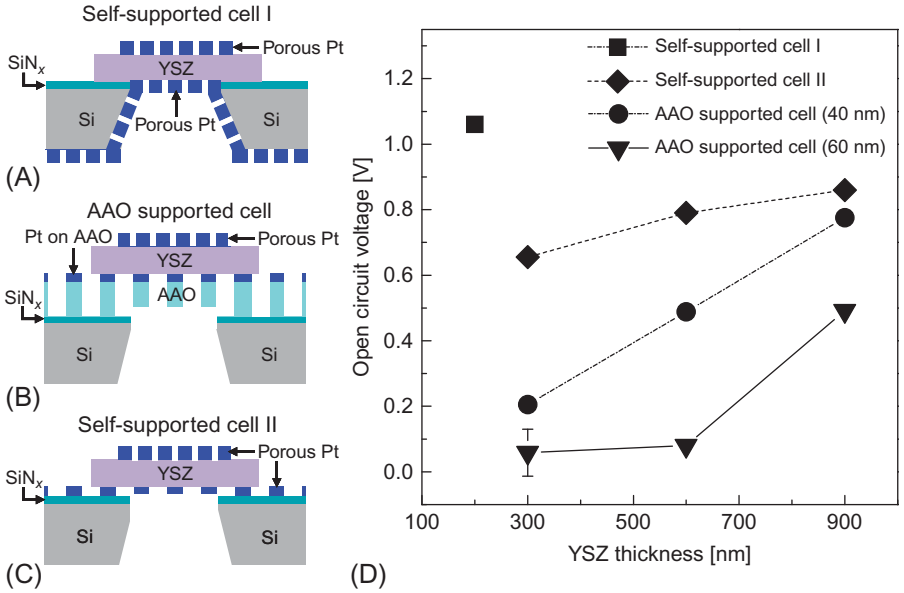

Fig. 15.9 (A)–(C) Schematic diagrams of the cell structures and the open-circuit voltages (OCVs) of the cells on various substrates as a function of YSZ thickness (D) [40].
Reproduced with permission from C.-W. Kwon, J.-W. Son, J.-H. Lee, H.-M. Kim, H.-W. Lee, K.-B. Kim, Adv. Funct. Mater. 21 (2011) 1154–1159, Copyright (2011) John Wiley and Sons.

One method to resolve the problem is to block the pinholes in the electrolyte by a conformal deposition like atomic layer deposition (ALD) [40,41]. In Fig. 15.10, the idea of blocking the pinholes by mixing the deposition techniques and the results are demonstrated [40]. When the first YSZ layer is deposited over the porous surface, then the inverted cone shaped grains are grown; and pinholes in between those grains are

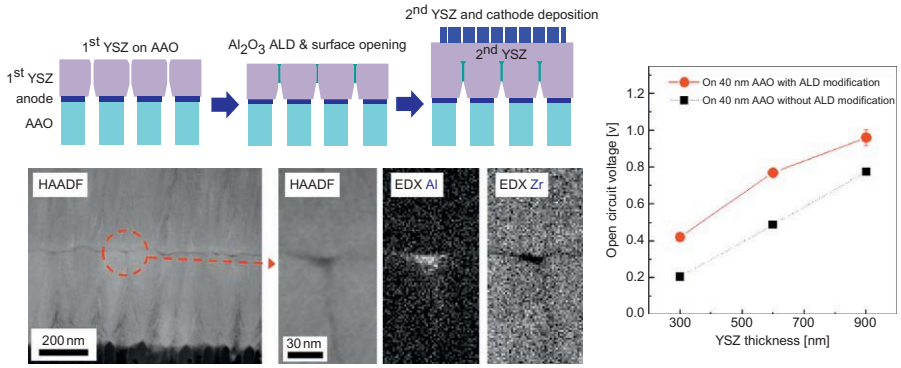

Fig. 15.10 Process flow to plug the pinholes in the electrolyte by ALD coating. Images showing the Al_2O_3 plugging the pinhole existing where inverted cone grains meet and OCV value change after the ALD modification [40].
Reproduced with permission from C.-W. Kwon, J.-W. Son, J.-H. Lee, H.-M. Kim, H.-W. Lee, K.-B. Kim, Adv. Funct. Mater. 21 (2011) 1154–1159, Copyright (2011) John Wiley and Sons.

unavoidable, as shown in the first schematic of Fig. 15.10. When ALD of a metal oxide thin film, in this case Al_2O_3, is deposited, then the entire surface and the pinholes are covered by Al_2O_3. As Al_2O_3 is an insulator, the Al_2O_3 layer covering the surface is removed and only the Al_2O_3 part plugging the pinhole is retained. In the case shown in Fig. 15.10, an additional (second) YSZ layer is deposited on the surface after the removal of ALD Al_2O_3, then a cathode layer is deposited subsequently to complete a unit cell. The second YSZ layer can be omitted. As can be seen in the OCV value change, this approach is successful in reducing the pinholes and gas leakage occurs there. After the method of the electrolyte thin film deposition by ALD is set, the electrolyte thin films are directly deposited by ALD over PVD electrolyte layers [41], which can exclude the processing step to remove the surface insulating layer and the additional electrolyte deposition.

If fabricated properly, the micro-SOFC can yield high OCVs $\sim$ 1 V and peak power density over 1 W/cm^2 at temperatures $\leq$500°C [34,42,43], which is comparable with that of conventional anode-supported SOFC around 700–800°C. The operating temperature of the SOFC can be lowered by 200–300°C to obtain the competitive cell performance by using this approach. It can be asserted that this MEMS-based micro-SOFC technology have proven the potential and provided a platform of LT-SOFCs of high performance with metal oxide thin films [44].

Nonetheless, there are significant issues remaining in micro-SOFCs to be used as practical devices. One is the scalability, that is, increasing the area of the unit cell. The micro-SOFCs fabricated on the Si substrate by KOH wet etching will lose substantial cell area because Si is etched with 54.7° with respect to (100) plane, so the resulting cell area is much smaller than the etched area starting at bottom of the substrate [32,44]. Moreover, the poor mechanical strength of the free-standing membrane hampers reliable production and operation of the cell. The membrane ruptures very easily depending on the temperature, fabrication methods, membrane size, electrolyte

thickness, mechanical shock, etc. [45–47]. As mentioned briefly, supporting structures to augment the mechanical stability of the free-standing membrane have been researched [37–39,47], but the fabrication complexity increase, lower OCV values as a price of the larger membrane, and tremendous decrease of the power density due to the absence of the proper lateral current collection method occurred. Until recently, the highest total power output from the micro-SOFC is only 21.1 mW from 25 mm^2 active area at 510°C [38].

The other is the extremely poor stability of the nanoporous metal electrodes, in general Pt. The Pt electrodes of micro-SOFCs are generally deposited by sputtering at high ambient pressure over 10 Pa to scatter intentionally the Pt deposit while traveling to the deposition surface, in this case the surface of the electrolyte, to reduce the density of the film for generating nanoporous structures. At an elevated temperature, although it is a very low temperature for the SOFC as 300–500°C, the nanoporous Pt agglomerates and dewets quickly at the surface of the electrolyte. To a certain extent, this is essential to produce the pores in the Pt films to produce triple-phase boundaries (TPB, electrolyte-electrode-gas-phase interface) [48]. However, after a very short duration, Pt agglomerates and the interconnectivity of the Pt is lost, and the cell performance deteriorates to an unacceptable level [43,47]. Most of the micro-SOFCs lose more than 20% of their peak power performance in less than an hour [39]. In Fig. 15.11 an example is presented. It was reported that the power density of the micro-SOFC with porous Pt electrodes reduced by 50% at 400°C, only after 12 h [43]. The study that demonstrated the highest performance of the micro-SOFC (1.3 W/cm^2 at 450°C) reported 30% of performance drop only after 3 h at 450°C as well [34]. Alloying of the metal electrode [49], using a combination of a nanoporous supporting structure (AAO) and a dense Pt film [47], coating the nanoporous Pt with an ultrathin oxide layer [50,51] have demonstrated effectiveness in retarding the structural degradation of the Pt, but more significant improvement is required in terms of the device lifetime.

15.7 LT-SOFCs fabricated over porous supports

As mentioned in Section 15.5, it is highly challenging to obtain gas-impermeable and thin electrolytes deposited over conventional porous supports of the SOFC. Micro-SOFCs discussed in Section 15.6 avoided this problem by depositing the ultrathin electrolyte over a perfectly dense surface of a substrate, but the lack of scalability, mechanical stability, and durability of the MEMS-based micro-SOFC hamper the practical usage of the technology.

An approach to resolve both problems is to modify the surface of the porous support to become appropriate to deposit dense electrolyte over it. If the pore sizes at the surface of the porous support is sufficiently small, then the pinholes generated in the electrolyte can be blocked with a relatively lesser thickness (see Fig. 15.8). The original pore size of the support can be reduced by metal electrode deposition in between the support and the electrolyte [52,53], or inserting nanoporous structure by a replication [54]. Still, rather thick electrolytes of a few microns were formed and even with this thickness, complete prevention of the pinholes in the electrolyte

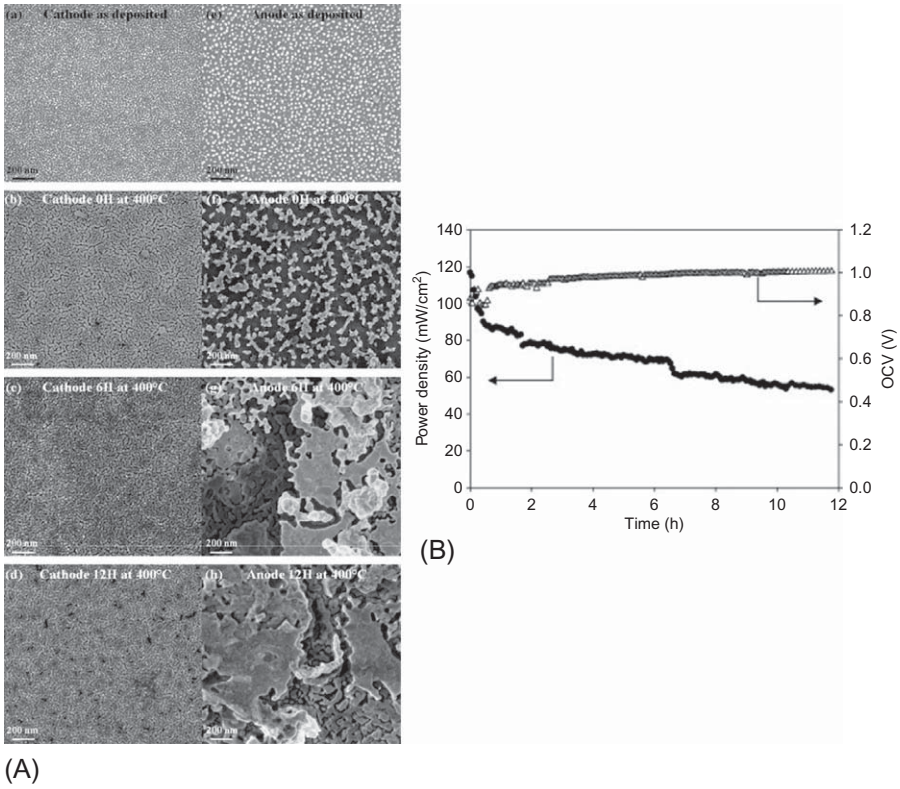

Fig. 15.11 (A) SEM micrographs of the cathode and anode as-deposited, heated up to 400°C, 6 h at 400°C, and 12 h at 400°C. (B) Overall performance and OCV of a Pt/YSZ/Pt micro-SOFC at 400°C operating continuously for 12 h with 5% wet H_2 as fuel. Open and closed symbols are for voltage and power density, respectively [43].
Reproduced with permission from K. Kerman, B.-K. Lai, S. Ramanathan, J. Power Sources 196 (2011) 2608–2614, Copyright (2011) Elsevier.

appeared to be difficult in these approaches because full OCVs were not obtained. The interfacial strength between the metal electrode and the metal oxide electrolyte can be weak, which can be another reason damaging the structural integrity of the electrolyte.

It appears that the dense surface of the substrate is essential to secure the desirable structure of the deposited electrolyte. But in this case, while not using the MEMS approach, how the bottom electrode structure which is porous and structurally support the electrolyte at the same time can be obtained?

One solution is to use an electrode support which is dense when the electrolyte is deposited, then transforms to be porous while the SOFC operation. One example is the SOFC cell developed in Kyushu University by using the Ni-Fe bimetal alloy as the substrate of PLD-deposited Sr and Mg-doped $LaGaO_3$ (LSGM) electrolyte [55]. A dense sintered body of NiO-Fe_2O_3 from Fe_2O_3-coated NiO powder was prepared

for the anode substrate of the electrolyte deposition. During in situ reduction of the anode substrate prior to the cell operation, NiO-Fe_2O_3 reduces to Ni-Fe and the volumetric change due to the reduction left micropores, while the structure of the deposited electrolyte was kept intact. Although the thickness of the electrolyte is rather more (~6 μm), high OCV and performance were obtained. However, in this approach, the electrolyte delamination was observed depending on the reduction condition, which is suspected to originate from the weak interfacial strength between the metal electrode and the metal oxide electrolyte. Another concern is that the small pore size is kept the same throughout the entire thickness of the support, which can significantly hamper gas diffusion at the support.

The examples shown above suggest following conditions for successfully fabricating thin and dense electrolyte over a porous support:

1. The surface of the porous support should be modified to be sufficiently dense for the thin and gas-impermeable electrolyte deposition.
2. The dense surface layer of the substrate should function as electrode, and should be porous during the SOFC operation.
3. The dense surface layer better not be pure metal to secure the interfacial bonding with the metal oxide electrolyte.
4. Except for the surface layer, the main volume of the support needs to be sufficiently porous not to impede gas transport.

One candidate for the surface layer can be the anode material of the SOFC. Between the two types of the electrode-supported cell shown in Fig. 15.2, anode-supported cells are preferred for lower-temperature operation because the resistance of the anode is generally lower than that of the cathode at low temperatures. Therefore, for the LT-SOFC, an anode is a natural choice of a support material. Thus, for the material compatibility, if a dense surface layer of the anode support can be constructed then the above-mentioned conditions can be satisfied.

The most adopted anode is the composite of the catalyst metal, most commonly Ni, and the electrolyte material, most commonly YSZ and other doped zirconia and doped ceria, for securing both electronic and ionic conductivity, catalytic activity, and material similarity with the electrolyte for interfacial adhesion and thermal expansion coefficient matching. There have been efforts to deposit NiO-electrolyte composite thin films [56–60], and by using thin film deposition, highly dense thin films of NiO-electrolyte composite can be obtained, which can be a proper surface modification layer of the porous support, as shown in Fig. 15.12A.

However, using as-deposited NiO-electrolyte composite layer as the anode of LT-SOFCs were largely unsuccessful because of the rapid agglomeration of Ni on reduction [57–59]. This is because of too fine size of Ni as shown in Fig. 15.12B, which is only several nm at best, and this fine-sized Ni has huge driving force for the agglomeration. The driving force of reducing the surface area of the reduced Ni is so substantial that the Ni particles with size reaching micron scale are produced on reduction, as shown in Fig. 15.12C and D. It appears that the Ni agglomeration is somewhat mitigated when the deposited films are not perfectly dense [58,60], but the complete understanding of the reason and prevention methods are not yet clear.

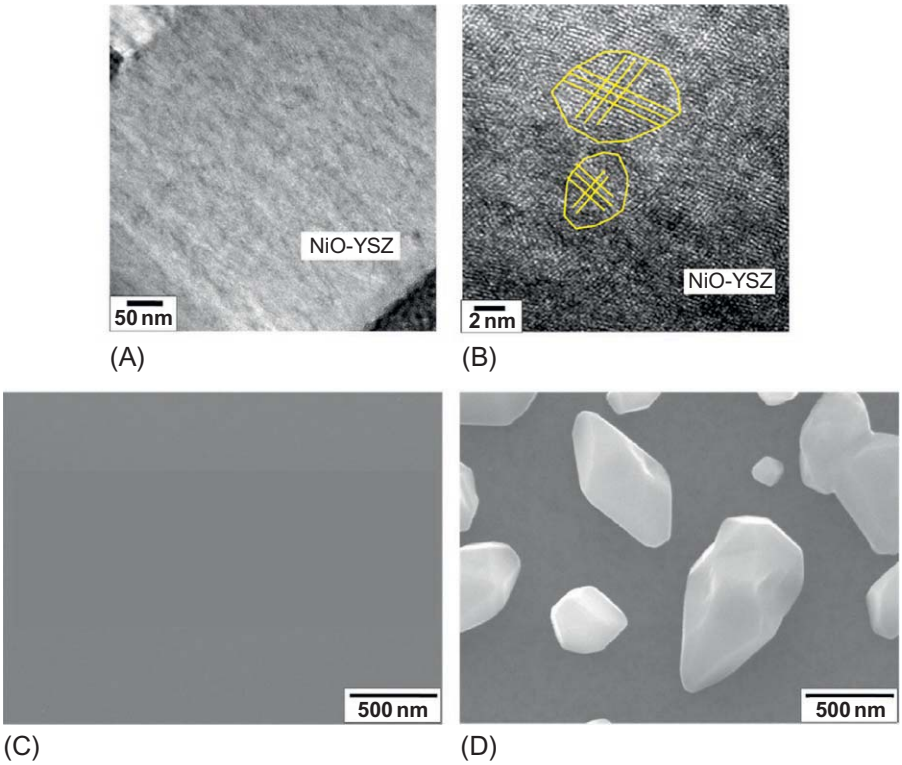

Fig. 15.12 (A) TEM and (B) high-resolution TEM micrographs of NiO-YSZ (40 vol% Ni after reduction) film deposited at 700°C in ambient oxygen pressure of 6.67 Pa (50 mTorr). SEM surface morphologies of the NiO-YSZ film: (C) as deposited; and (D) after 500°C 1-h reduction in 4% H_2 [59].
Reproduced with permission from H.-S. Noh, J.-S. Park, J.-W. Son, H. Lee, J.-H. Lee, H.-W. Lee, J. Am. Ceram. Soc. 92 (2009) 3059–3064, Copyright (2009) John Wiley and Sons.

If this layer is used as the surface modification layer of the porous anode support, then the Ni agglomeration would destroy the thin film components over it [61]. In Fig. 15.13, a case of using the as-deposited anode composite thin film as the surface modification layer of the porous substrate is displayed. An electrolyte layer and a cathode layer were formed over the deposited NiO-YSZ layer and after the reduction for the cell operation, it was found that the whole electrolyte-cathode layers were lifted by the Ni agglomeration at the NiO-YSZ layer. A proper OCV value was not obtained for this cell and the cell performance measurement was not possible [61].

As the minute particle size of NiO and the resulting tiny size of Ni is the main reason of the excessive agglomeration, a solution to avoid this phenomenon is to intentionally grow the grain size of NiO. Muecke et al. [58] reported a systematic study based on spray pyrolysis Ni/NiO-GDC thin films as a function of the grain size of the composite. If the grain size is too small and the GDC particles are not well sintered

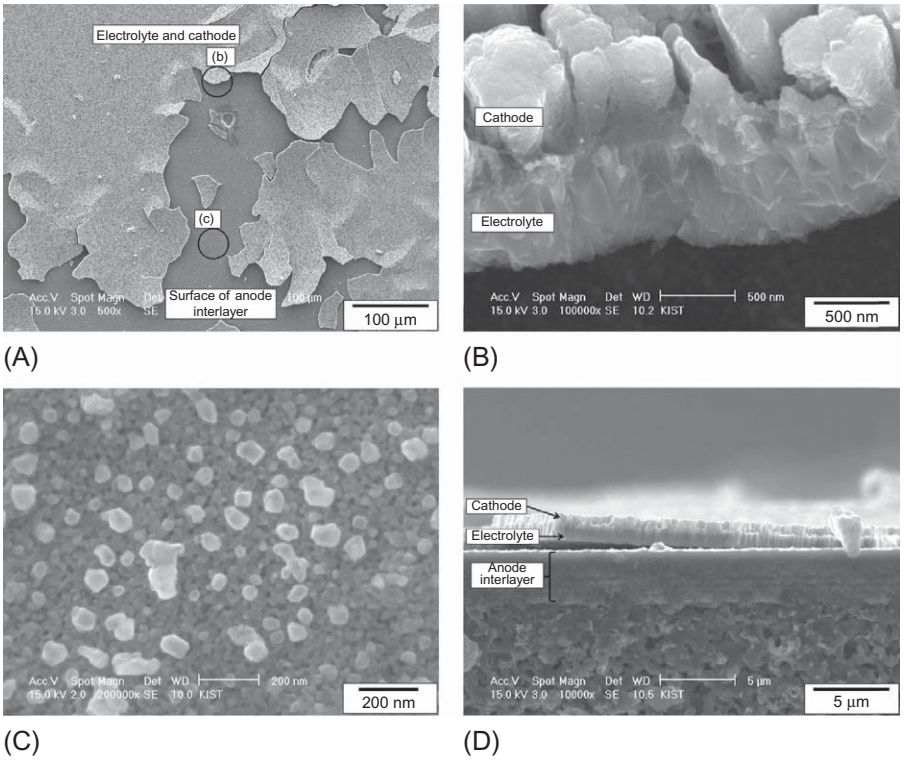

Fig. 15.13 (A) Low magnification picture of the surface of the cell with NiO-YSZ interlayer without postannealing after cell test. (B) Image of delaminated layers [area marked (b) in (a)]. (C) Ni agglomerates observed underneath delaminated electrolyte layer [area marked (c) in (a)]. (D) Cross-sectional micrograph showing delaminated electrolyte-cathode layer and relatively dense interlayer [61].
Reproduced with permission from H.-S. Noh, J.-W. Son, H. Lee, H.-S. Song, H.-W. Lee, J.-H. Lee, J. Electrochem. Soc. 156 (2009) B1484–B1490, Copyright (2009) The Electrochemical Society.

together, the driving force to reduce the surface area of the Ni is huge and gigantic Ni agglomerates would form and destroy the weak ceramic network. The stability of the ceramic (in this case of GDC) network would be strengthened and the surface area of the Ni would be reduced by intentional grain growth by postannealing at higher temperatures. The abnormal coarsening of Ni can be prohibited during the reduction by both a more rigid ceramic framework and a less driving force for Ni agglomeration. In Fig. 15.14, a schematic is presented based on the results of this study [58].

One disadvantage of the postannealing of the anode composite is that this cannot be applied after the thin film electrolyte is deposited such as micro-SOFCs, because thin film electrolyte cannot sustain its structure at the postannealing temperature. For the modification of the surface of the porous support like anode supports, however, it is a

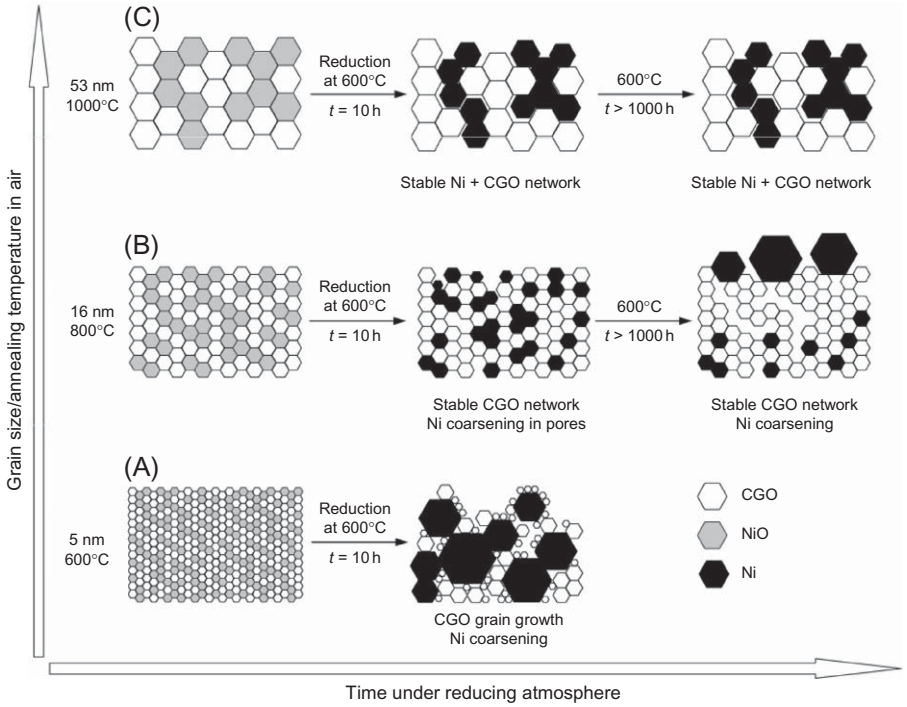

Fig. 15.14 Schematic representation of the different morphologies of nanocrystalline NiO-GDC (i.e., CGO) films and Ni-GDC cermets as a function of grain size and operating times [58].
Reproduced with permission from U.P. Muecke, S. Graf, U. Rhyner, L.J. Gauckler, Acta Mater. 56 (2008) 677–687, Copyright (2008) Elsevier.

very appropriate solution as long as a dense anode thin film layer can be fabricated. It will satisfy the 1–4 conditions listed earlier, and the material compatibility with the anode support is perfect, and that with the electrolyte is descent. When the anode composite is deposited by PVD, almost perfectly dense films can be formed as shown in Fig. 15.12A, unlike spray-based methods [59]. It was also found that when the composite film was deposited, each component disturbed each other so the grain structures of each were equiaxed, not columnar, as shown in Fig. 15.12B [59]. After postannealing, it was found that the grain growth of each component occurred and interconnected networks with enlarged grains were formed [62]. By changing the postannealing temperature, the grain size can be controlled and as grain grows to a ~100-nm level, no excessive agglomeration of Ni on reduction was observed, as shown in Fig. 15.15. The TPB density of this structure was found to be almost 20 times higher than that of the powder-processed anode due to the fine particle size [16], and plays a key role in securing the low-temperature performance by reducing the resistance originating from the anode-electrolyte interface, owing to the increased TPB density [17].

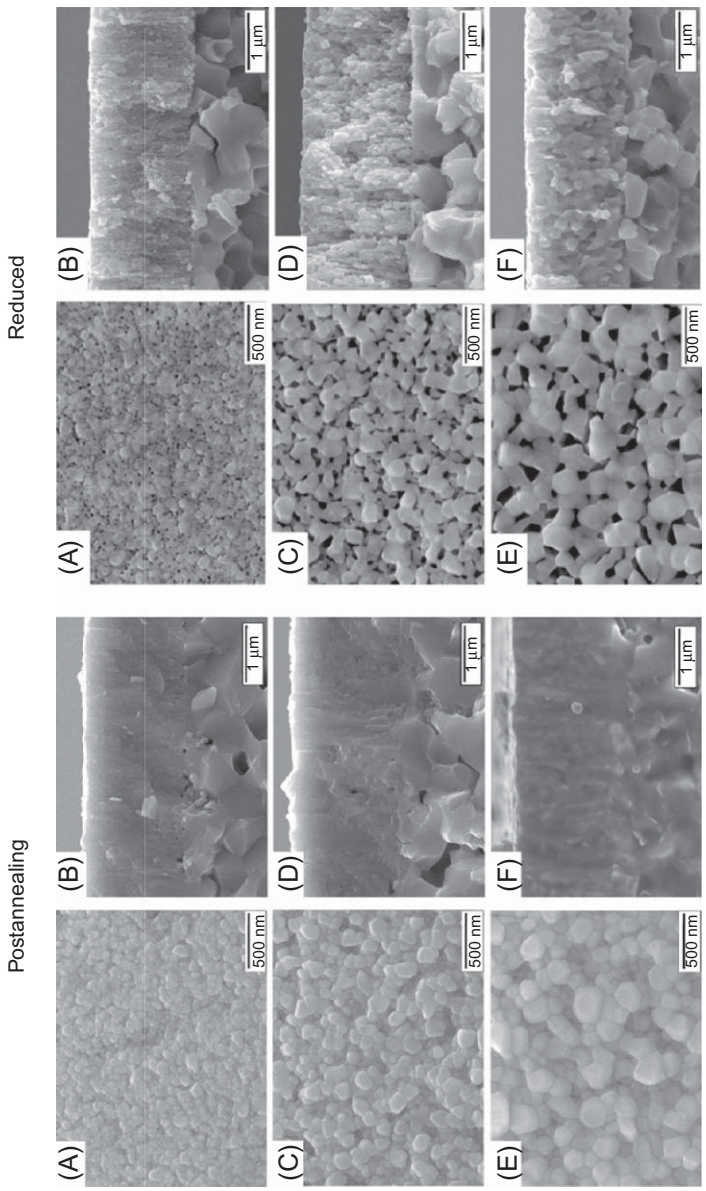

Fig. 15.15 Surface and cross-sectional morphologies of postannealed (left) and reduced (right) NiO–YSZ anode composite thin films deposited by PLD [62].
Reproduced with permission from H.-S. Noh, J.-W. Son, H. Lee, H.-I. Ji, J.-H. Lee, H.-W. Lee, J. Eur. Ceram. Soc. 30 (2010) 3415–3423, Copyright (2010) Elsevier.

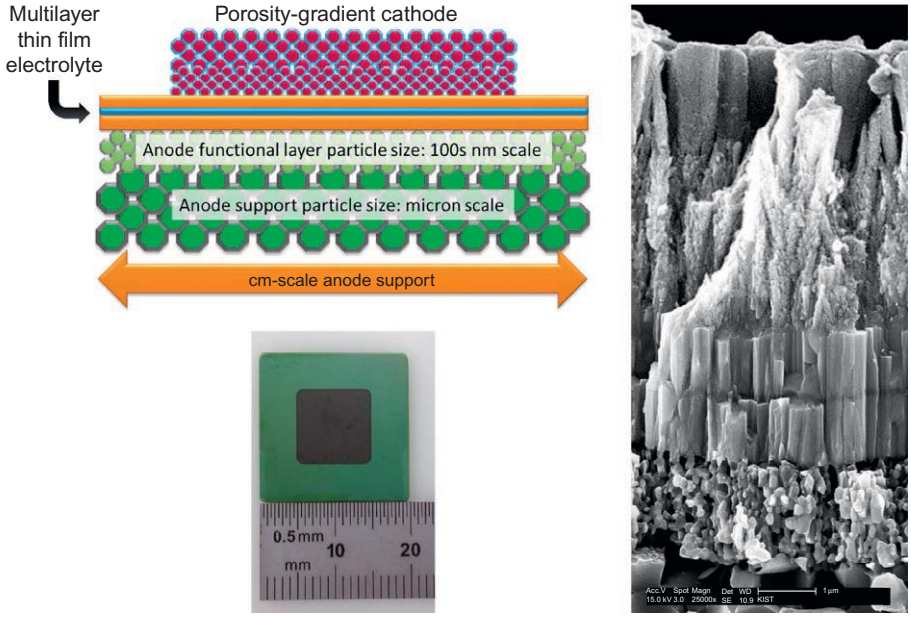

Fig. 15.16 A schematic, a digital picture, and an SEM micrograph of a fabricated multiscale-architectured LT-SOFC.

Based on this layer, the interface structure control at the porous anode support and the thin electrolyte became possible. The thin film-based LT-SOFC constructed on this structure is called "multiscale-architectured" thin film SOFC because various marco-micro-nano structural scale levels are contained in this cell platform [63]. In Fig. 15.16, a schematic, a digital picture, and an SEM micrograph of an exemplary 2 cm × 2 cm multiscale-architectured LT-SOFC are displayed.

The multiscale-architectured LT-SOFC has following characteristics:

1. Owing to the surface modification of the anode support with a dense and nanostructure anode composite layer as shown in Fig. 15.16 on the left hand side, the OCV can reach almost the theoretical value, which indicates that the thin and gas-impermeable electrolytes can be deposited [62]. The dense nanostructure anode layer transforms into a porous layer during reduction, which is prior to the initiation of the cell operation [62,64], thus functions properly as a porous anode.
2. The maximum power density of the cell using conventional SOFC materials has reached above 2 W/cm^2 at 650°C and about 0.6 W/cm^2 at 500°C [65]. This performance is about 3–4 times higher than that of powder-processed HT-SOFCs based on the same materials at the same operation temperature. See Fig. 15.17A and B.
3. The multiscale-architectured LT-SOFC can produce a comparable cell performance to that of the HT-SOFC at about 150°C lower operation temperature, which demonstrates the impact of the reduction of the physical dimensions of cell components by metal oxide thin film technology. See Fig. 15.17C.

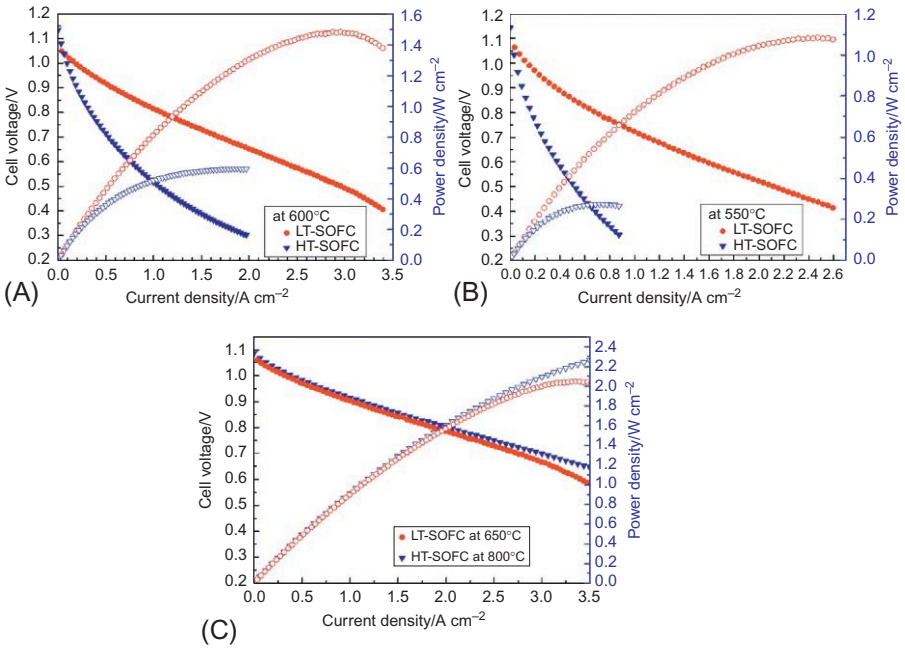

Fig. 15.17 Current density-voltage-power (I-V-P) curve comparison between LT-SOFC [65] and HT-SOFC [77]. Both LT-SOFC and HT-SOFC were constructed using the same materials: Ni-YSZ anode, YSZ/GDC bilayer electrolyte, LSC-GDC, and LSC cathode. Cell performance comparison (A) at 600°C and (B) 550°C. (C) I-V-P curves obtained at temperatures where the comparable cell performances were obtained, LT-SOFC at 650°C and HT-SOFC at 800°C.

4. The thermomechanical stability is superior to that of micro-SOFCs due to the multiscale support. It can sustain more than 50 times of thermal cycling and in spite of the cycling, the cell performance degradation was only 17%/100 h [63]. Under the constant load condition, the cell degradation does not exceed 1%/100 h at 450°C.
5. The scalability of the cell can be attainable to significantly larger area. It was demonstrated that a 5 cm × 5 cm multiscale-architectured cell can be fabricated by using a 2-in. sputtering system [66]. Much larger substrates can be held by a bigger sputtering apparatus and if the deposition ratio of the complex metal oxides and composites can be secured, then it is expected that larger area cell fabrication can be easily achievable.
6. Various SOFC electrolyte materials, YSZ/GDC [61,65,67–69], LSGM [70]; cathode materials like single-phase LSC and LSC-GDC nanocomposites [71–73] can be easily integrated over the multiscale anode support.
7. Even at the anode side, material flexibility can be achieved owing to the thin film deposition. Incorporating heterogeneous catalysts at the nanostructure anode functional layer (fuel electrode), nearby the fuel electrode, and the electrolyte interface is possible by multiple layer depositions [74].
8. Recently, a successful fabrication of a PCFC with doped $BaZrO_3$ thin-film electrolyte built over multiscale proton-conducting anode supports was demonstrated as well, in spite of the difficulties of the handling and processing of the doped $BaZrO_3$ [75]. In addition, even a

PCFC can be constructed over an SOFC anode support based on this technology, in spite of the material dissimilarity [76].

9. The characteristic 8 and 9, that is, various material combinations, is possible because the cell components of multiscale-architectured LT-SOFCs are fabricated by thin film deposition. After a surface-modified multiscale anode is fabricated as a rigid substrate, the metal oxide thin film components are deposited at much lower temperatures than that of the sintering temperature, which eliminates the problems related to the sintering shrinkage and the undesirable chemical reaction accompanying the high-temperature sintering.

In all, the multiscale-architectured thin film-based LT-SOFC can be a representative example, which demonstrates the importance of the proper interface structure modification between the porous support and the thin film electrolyte for obtaining an LT-SOFC not only with high performance but also with reasonable stability. In addition, it demonstrates the impact of the thin film and nanostructures for the operating temperature reduction of the SOFC, as well as the advantage of the thin film processing when properly used. Although much further research and development are required to construct an integrated LT-SOFC system with long-term stability for practical applications, this cell platform shows promising potentials at the unit cell level in comparison with other competing technologies.

15.8 Concluding remarks

In this chapter, efforts to lower the operating temperature of SOFCs by using metal oxide thin film technology and interface control is discussed. The advantages of the SOFC can be retained, whereas the disadvantages like fast degradation and poor reliability can be effectively overcome if the metal oxide thin film technology is properly utilized to lower the operating temperature of the SOFC without compromising the cell performance. However, interfacial structure control to suppress instability of the thin electrolyte and nanostructure electrodes at an elevated temperature should be seriously considered to realize an LT-SOFC, which can be reliably applicable to real devices. Especially, the most important prerequisite is to realize a dense, gas-impermeable thin film metal oxide electrolyte over porous electrode structures. Here, an example of such a cell platform, the multiscale-architectured thin-film-based LT-SOFC, is introduced. Although this platform demonstrated the potential of a thin-film-based LT-SOFC with high performance and improved stability, there still remain many tasks to further mitigate the intrinsic weakness of the thin film and nanostructures at the operating temperature of the LT-SOFC. Provided these issues are resolved, the possible applications of the SOFC technology will be expanded to the greatly integrated high-energy density power sources of which the need is ever increasing for the portable and mobile applications such as unmanned aerial, ground, undersea vehicles, robots, and electric cars, as well as for the conventional SOFC usages.

Acknowledgments

I thank my coworkers, and former and present students at High-temperature Energy Materials Research Center at KIST for their excellent work and collaboration on thin film-based

LT-SOFC. I also appreciate the financial support from the Global Frontier R&D Program on Center for Multiscale Energy Systems (Grant No. NRF-2015M3A6A7065442) of the National Research Foundation (NRF) of Korea funded by the Ministry of Science, ICT & Future Planning (MSIP), and to the Institutional Research Program of KIST, which enable sustainable research on the LT-SOFC.

References

[1] H.Y. Jung, S.H. Choi, H. Kim, J.W. Son, J. Kim, H.W. Lee, J.H. Lee, Fabrication and performance evaluation of 3-cell SOFC stack based on planar 10 cm × 10 cm anode-supported cells, J. Power Sources 159 (2006) 478–483.
[2] E.D. Wachsman, K.T. Lee, Lowering the temperature of solid oxide fuel cells, Science 334 (2011) 935–939.
[3] B.C.H. Steele, A. Heinzel, Materials for fuel-cell technologies, Nature 414 (2001) 345–352.
[4] Z. Gao, L.V. Mogni, E.C. Miller, J.G. Railsback, S.A. Barnett, A perspective on low-temperature solid oxide fuel cells, Energ. Environ. Sci. 9 (2016) 1602–1644.
[5] Assessment of Plarnar Solid Oxide Fuel Cell Technology, DOE Report, Arthur D. Little, 1999.
[6] M.R. Weimar, L.A. Chick, D.W. Gotthold, G.A. Whyatt, Cost Study for Manufacturing of Solid Oxide Fuel Cell Power Systems, DOE Report, PNNL, 2013.
[7] http://arpa-e.energy.gov/?q=programs/rebels.
[8] R. O'Hayer, S. Cha, W. Colella, F.B. Prinz, Fuel Cell Fundamentals, John Wiley & Sons, New York, 2006.
[9] H.-G. Jung, Y.-K. Sun, H.-Y. Jung, J.-S. Park, H.-R. Kim, G.-H. Kim, H.-W. Lee, J.-H. Lee, Investigation of anode-supported SOFC with cobalt-containing cathode and GDC interlayer, Solid State Ionics 179 (2008) 1535–1539.
[10] A. Aguadero, L. Fawcett, S. Taub, R. Woolley, K.-T. Wu, N. Xu, J.A. Kilner, S.J. Skinner, Materials development for intermediate-temperature solid oxide electrochemical devices, J. Mater. Sci. 47 (2012) 3925–3948.
[11] J.S. Ahn, D. Pergolesi, M.A. Camaratta, H. Yoon, B.W. Lee, K.T. Lee, D.W. Jung, E. Traversa, E.D. Wachsman, High-performance bilayered electrolyte intermediate temperature solid oxide fuel cells, Electrochem. Commun. 11 (2009) 1504–1507.
[12] S. Choi, S. Yoo, J. Kim, S. Park, A. Jun, S. Sengodan, J. Kim, J. Shin, H.Y. Jeong, Y. Choi, G. Kim, M. Liu, Highly efficient and robust cathode materials for low-temperature solid oxide fuel cells: PrBa0.5Sr0.5Co2−xFexO5+δ, Sci. Rep. 3 (2013) 2426.
[13] J. Hayd, L. Dieterle, U. Guntow, D. Gerthsen, E. Ivers-Tiffée, Nanoscaled $La_{0.6}Sr_{0.4}CoO_{3-d}$ as intermediate temperature solid oxide fuel cell cathode: microstructure and electrochemical performance, J. Power Sources 196 (2011) 7263–7270.
[14] C. Peters, A. Weber, E. Ivers-Tiffee, Nanoscaled $(La_{0.5}Sr_{0.5})CoO_{3-d}$ thin film cathodes for SOFC application at 500°C < T < 700°C, J. Electrochem. Soc. 155 (2008) B730–B737.
[15] J. Joos, M. Ender, T. Carraro, A. Weber, E. Ivers-Tiffée, Representative volume element size for accurate solid oxide fuel cell cathode reconstructions from focused ion beam tomography data, Electrochim. Acta 82 (2012) 268–276.
[16] D. Kennouche, J. Hong, H.-S. Noh, J.-W. Son, S.A. Barnett, Three-dimensional microstructure of high-performance pulsed-laser deposited Ni-YSZ SOFC anodes, Phys. Chem. Chem. Phys. 16 (2014) 15249–15255.

[17] J.H. Park, S.M. Han, K.J. Yoon, H. Kim, J. Hong, B.-K. Kim, J.-H. Lee, J.-W. Son, Impact of nanostructured anode on low-temperature performance of thin-film-based anode-supported solid oxide fuel cells, J. Power Sources 315 (2016) 324–330.
[18] N. Sata, K. Eberman, K. Eberl, J. Maier, Mesoscopic fast ion conduction in nanometer-scale planar heterostructures, Nature 408 (2000) 946–949.
[19] A. Peters, C. Korte, D. Hesse, N. Zakharov, J. Janek, Ionic conductivity and activation energy for oxygen ion transport in superlattices—the multilayer system CSZ (ZrO_2+CaO)/Al_2O_3, Solid State Ionics 178 (2007) 67–76.
[20] N. Schichtel, C. Korte, D. Hesse, J. Janek, Eleactic strain at interfaces and its infuluence on ionic conductivity in nanoscaled solid electrolyte thin films—theoretical considerations and experimental studies, Phys. Chem. Chem. Phys. 11 (2009) 3043–3048.
[21] J. Garcia-Barriocanal, A. Rivera-Calzada, M. Varela, Z. Sefrioui, E. Iborra, C. Leon, S.J. Pennycook, J. Santamaria, Colossal ionic conductivity at interfaces of epitaxial ZrO_2:Y_2O_3/$SrTiO_3$ heterostructures, Science 321 (2008) 676–680.
[22] M. Yano, A. Tomita, M. Sano, T. Hibino, Recent advances in single-chamber solid oxide fuel cells: a review, Solid State Ionics 177 (2007) 3351–3359.
[23] S.-J. Ahn, Y.-B. Kim, J. Moon, J.-H. Lee, J. Kim, Co-planar type single chamber solid oxide fuel cell with micro-patterned electrodes, J. Electroceram. 17 (2006) 689–693.
[24] J. Yoon, S. Cho, J.-H. Kim, J. Lee, Z. Bi, A. Serquis, X. Zhang, A. Manthiram, H. Wang, Vertically aligned nanocomposite thin films as a cathode/electrolyte interface layer for thin-film solid oxide fuel cells, Adv. Funct. Mater. 19 (2009) 3868–3873.
[25] W. Ma, J.J. Kim, N. Tsvetkov, T. Daio, Y. Kuru, Z. Cai, Y. Chen, K. Sasaki, H.L. Tuller, B. Yildiz, Vertically aligned nanocomposite La0.8Sr0.2CoO3/(La0.5Sr0.5)2CoO4 cathodes—electronic structure, surface chemistry and oxygen reduction kinetics, J. Mater. Chem. A 3 (2015) 207–219.
[26] T. Tsai, S.A. Barnett, Bias sputter deposition of dense yttria-stabilized zirconia fils on porous substrates, J. Electrochem. Soc. 142 (1995) 3084–3087.
[27] A. Nagata, H. Okayama, Characterization of solid oxide fuel cell device having a three-layer film structure grown by RF magnetron sputtering, Vacuum 66 (2002) 523–529.
[28] B. Hobein, F. Tietz, D. Stover, M. Cekada, P. Panjan, DC sputtering of yttria-stabilised zirconia films for solid oxide fuel cell applications, J. Eur. Ceram. Soc. 21 (2001) 1843–1846.
[29] H.-Y. Jung, K.-S. Hong, H. Kim, J.-K. Park, J.-W. Son, J. Kim, H.-W. Lee, J.-H. Lee, Characterization of thin-film YSZ deposited via EB-PVD technique in anode-supported SOFCs, J. Electrochem. Soc. 153 (2006) A961–A966.
[30] H. Huang, M. Nakamura, P.C. Su, R. Fasching, Y. Saito, F.B. Prinz, High-performance ultrathin solid oxide fuel cells for low-temperature operation, J. Electrochem. Soc. 154 (2007) B20–B24.
[31] J.H. Shim, J.S. Park, J. An, T.M. Gür, S. Kang, F.B. Prinz, Intermediate-temperature ceramic fuel cells with thin film yttrium-doped barium zirconate electrolytes, Chem. Mater. 21 (2009) 3290–3296.
[32] P.C. Su, C.C. Chao, J.H. Shim, R. Fasching, F.B. Prinz, Solid oxide fuel cell with corrugated thin film electrolyte, Nano Lett. 8 (2008) 2289–2292.
[33] Y.B. Kim, T.M. Gür, S. Kang, H.-J. Jung, R. Sinclair, F.B. Prinz, Crater patterned 3-D proton conducting ceramic fuel cell architecture with ultra thin Y:BaZrO3 electrolyte, Electrochem. Commun. 13 (2011) 403–406.
[34] J. An, Y.-B. Kim, J. Park, T.M. Gür, F.B. Prinz, Three-dimensional nanostructured bilayer solid oxide fuel cell with 1.3 W/cm^2 at 450°C, Nano Lett. 13 (2013) 4551–4555.

[35] C.-C. Chao, C.-M. Hsu, Y. Cui, F.B. Prinz, Improved solid oxide fuel cell performance with nanostructured electrolytes, ACS Nano 5 (2011) 5692–5696.
[36] U.P. Muecke, D. Beckel, A. Bernard, A. Bieberle-Hutter, S. Graf, A. Infortuna, P. Muller, J.L.M. Rupp, J. Schneider, L.J. Gauckler, Micro solid oxide fuel cells on glass ceramic substrates, Adv. Funct. Mater. 18 (2008) 3158–3168.
[37] S. Rey-Mermet, P. Muralt, Solid oxide fuel cell membranes supported by nickel grid anode, Solid State Ionics 179 (2008) 1497–1500.
[38] M. Tsuchiya, B.-K. Lai, S. Ramanathan, Scalable nanostructured membranes for solid-oxide fuel cells, Nat. Nano 6 (2011) 282–286.
[39] I. Garbayo, D. Pla, A. Morata, L. Fonseca, N. Sabate, A. Tarancon, Full ceramic micro solid oxide fuel cells: towards more reliable MEMS power generators operating at high temperatures, Energ. Environ. Sci. 7 (2014) 3617–3629.
[40] C.-W. Kwon, J.-W. Son, J.-H. Lee, H.-M. Kim, H.-W. Lee, K.-B. Kim, High-performance micro-solid oxide fuel cells fabricated on nanoporous anodic aluminum oxide templates, Adv. Funct. Mater. 21 (2011) 1154–1159.
[41] I. Chang, J. Bae, J. Park, S. Lee, M. Ban, T. Park, Y.H. Lee, H.H. Song, Y.-B. Kim, S.W. Cha, A thermally self-sustaining solid oxide fuel cell system at ultra-low operating temperature (319°C), Energy 104 (2016) 107–113.
[42] Z. Fan, J. An, A. Iancu, F.B. Prinz, Thickness effects of yttria-doped ceria interlayers on solid oxide fuel cells, J. Power Sources 218 (2012) 187–191.
[43] K. Kerman, B.-K. Lai, S. Ramanathan, Pt/$Y_{0.16}Zr_{0.84}O_{1.92}$/Pt thin film solid oxide fuel cells: electrode microstructure and stability considerations, J. Power Sources 196 (2011) 2608–2614.
[44] J. An, J.H. Shim, Y.-B. Kim, J.S. Park, W. Lee, T.M. Gür, F.B. Prinz, MEMS-based thin-film solid-oxide fuel cells, MRS Bull. 39 (2014) 798–804.
[45] C.D. Baertsch, K.F. Jensen, J.L. Hertz, H.L. Tuller, S.T. Vengallatore, S.M. Spearing, M.A. Schmidt, Fabrication and structural characterization of self-supporting electrolyte membranes for a micro solid-oxide fuel cell, J. Mater. Res. 19 (2004) 2604–2615.
[46] A. Evans, M. Prestat, R. Tölke, M.V.F. Schlupp, L.J. Gauckler, Y. Safa, T. Hocker, J. Courbat, D. Briand, N.F. de Rooij, D. Courty, Residual stress and buckling patterns of free-standing yttria-stabilized-zirconia membranes fabricated by pulsed laser deposition, Fuel Cells 12 (2012) 614–623.
[47] C.-W. Kwon, J.-I. Lee, K.-B. Kim, H.-W. Lee, J.-H. Lee, J.-W. Son, The thermomechanical stability of micro-solid oxide fuel cells fabricated on anodized aluminum oxide membranes, J. Power Sources 210 (2012) 178–183.
[48] T. Ryll, H. Galinski, L. Schlagenhauf, P. Elser, J.L.M. Rupp, A. Bieberle-Hutter, L.J. Gauckler, Microscopic and nanoscopic three-phase-boundaries of platinum thin-film electrodes on YSZ electrolyte, Adv. Funct. Mater. 21 (2011) 565–572.
[49] X.H. Wang, H. Huang, T. Holme, X. Tian, F.B. Prinz, Thermal stabilities of nanoporous metallic electrodes at elevated temperatures, J. Power Sources 175 (2008) 75–81.
[50] I. Chang, S. Ji, J. Park, M.H. Lee, S.W. Cha, Ultrathin YSZ coating on pt cathode for high thermal stability and enhanced oxygen reduction reaction activity, Adv. Energy Mater. 5 (2015) 1402251.
[51] K.-Y. Liu, L. Fan, C.-C. Yu, P.-C. Su, Thermal stability and performance enhancement of nano-porous platinum cathode in solid oxide fuel cells by nanoscale ZrO2 capping, Electrochem. Commun. 56 (2015) 65–69.
[52] S. Kang, P. Heo, Y.H. Lee, J. Ha, I. Chang, S.-W. Cha, Low intermediate temperature ceramic fuel cell with Y-doped BaZrO3 electrolyte and thin film Pd anode on porous substrate, Electrochem. Commun. 13 (2011) 374–377.

[53] J.H. Joo, G.M. Choi, Simple fabrication of micro-solid oxide fuel cell supported on metal substrate, J. Power Sources 182 (2008) 589–593.
[54] S. Kang, P.C. Su, Y.I. Park, Y. Saito, F.B. Prinz, Thin-film solid oxide fuel cells on porous nickel substrates with multistage nanohole array, J. Electrochem. Soc. 153 (2006) A554–A559.
[55] Y.-W. Ju, H. Eto, T. Inagaki, S. Ida, T. Ishihara, Preparation of Ni–Fe bimetallic porous anode support for solid oxide fuel cells using LaGaO3 based electrolyte film with high power density, J. Power Sources 195 (2010) 6294–6300.
[56] S. Jou, T.-H. Wu, Thin porous Ni–YSZ films as anodes for a solid oxide fuel cell, J. Phys. Chem. Solids 69 (2008) 2804–2812.
[57] T. Tsai, S.A. Barnett, Sputter deposition of cermet fuel electrodes for solid oxide fuel cells, J. Vac. Sci. Technol. A 13 (1995) 1073–1077.
[58] U.P. Muecke, S. Graf, U. Rhyner, L.J. Gauckler, Microstructure and electrical conductivity of nanocrystalline nickel- and nickel oxide/gadolinia-doped ceria thin films, Acta Mater. 56 (2008) 677–687.
[59] H.-S. Noh, J.-S. Park, J.-W. Son, H. Lee, J.-H. Lee, H.-W. Lee, Physical and microstructural properties of NiO- and Ni-YSZ composite thin films fabricated by pulsed laser deposition at $T \leq 700°C$, J. Am. Ceram. Soc. 92 (2009) 3059–3064.
[60] K.J. Kim, B.H. Park, S.J. Kim, Y. Lee, H. Bae, G.M. Choi, Micro solid oxide fuel cell fabricated on porous stainless steel: a new strategy for enhanced thermal cycling ability, Sci. Rep. 6 (2016) 22443.
[61] H.-S. Noh, J.-W. Son, H. Lee, H.-S. Song, H.-W. Lee, J.-H. Lee, Low temperature performance improvement of SOFC with thin film electrolyte and electrodes fabricated by pulsed laser deposition, J. Electrochem. Soc. 156 (2009) B1484–B1490.
[62] H.-S. Noh, J.-W. Son, H. Lee, H.-I. Ji, J.-H. Lee, H.-W. Lee, Suppression of Ni agglomeration in PLD fabricated Ni-YSZ composite for surface modification of SOFC anode, J. Eur. Ceram. Soc. 30 (2010) 3415–3423.
[63] H.-S. Noh, K.J. Yoon, B.-K. Kim, H.-J. Je, H.-W. Lee, J.-H. Lee, J.-W. Son, Thermomechanical stability of multi-scale-architectured thin-film-based solid oxide fuel cells assessed by thermal cycling tests, J. Power Sources 249 (2014) 125–130.
[64] H.-S. Noh, J.-S. Park, H. Lee, H.-W. Lee, J.-H. Lee, J.-W. Son, Transmission electron microscopy study on microstructure and interfacial property of thin film electrolyte SOFC, Elecrochem. Solid State Lett. 14 (2011) B26–B29.
[65] H.-S. Noh, K.J. Yoon, B.-K. Kim, H.-J. Je, H.-W. Lee, J.-H. Lee, J.-W. Son, The potential and challenges of thin-film electrolyte and nanostructured electrode for yttria-stabilized zirconia-base anode-supported solid oxide fuel cells, J. Power Sources 247 (2014) 105–111.
[66] H.-S. Noh, J. Hong, H. Kim, K.J. Yoon, B.-K. Kim, H.-W. Lee, J.-H. Lee, J.-W. Son, Scale-up of thin-film deposition-based solid oxide fuel cell by sputtering, a commercially viable thin-film technology, J. Electrochem. Soc. 163 (2016) F613–F617.
[67] H.-S. Noh, H. Lee, B.-K. Kim, H.-W. Lee, J.-H. Lee, J.-W. Son, Microstructural factors of electrodes affecting the performance of anode-supported thin film yttria-stabilized zirconia electrolyte ($\sim$1 mm) solid oxide fuel cells, J. Power Sources 196 (2011) 7169–7174.
[68] D.-H. Myung, J. Hong, K. Yoon, B.-K. Kim, H.-W. Lee, J.-H. Lee, J.-W. Son, The effect of an ultra-thin zirconia blocking layer on the performance of a 1-μm-thick gadolinia-doped ceria electrolyte solid-oxide fuel cell, J. Power Sources 206 (2012) 91–96.
[69] H.-S. Noh, K.J. Yoon, B.-K. Kim, H.-J. Je, H.-W. Lee, J.-H. Lee, J.-W. Son, Ultimate performance of anode-supported SOFC by realizing thin-film electrolyte and nano-structure electrode, ECS Trans. 57 (2013) 969–973.

[70] J. Hwang, H. Lee, J.-H. Lee, K.J. Yoon, H. Kim, J. Hong, J.-W. Son, Specific considerations for obtaining appropriate La1−xSrxGa1−yMgyO3−δ thin films using pulsed-laser deposition and its influence on the performance of solid-oxide fuel cells, J. Power Sources 274 (2015) 41–47.

[71] D.-H. Myung, J. Hwang, J. Hong, H.-W. Lee, B.-K. Kim, J.-H. Lee, J.-W. Son, Pulsed laser deposition of $La_{0.6}Sr_{0.4}CoO_{3-d}$-$Ce_{0.9}Gd_{0.1}O_{2-d}$ nano-composite and its application to gradient-structured thin-film cathode of SOFC, J. Electrochem. Soc. 158 (2011) B1000–B1006.

[72] J.-H. Park, W.-S. Hong, G.C. Kim, H.J. Chang, J.-H. Lee, K.J. Yoon, J.-W. Son, The effect of post-annealing on the properties of a pulsed-laser-deposited $La_{0.6}Sr_{0.4}CoO_{3-\delta}$-$Ce_{0.9}Gd_{0.1}O_{2-\delta}$ nano-composite cathode, J. Electrochem. Soc. 160 (2013) F1027–F1032.

[73] J.-H. Park, W.-S. Hong, K.J. Yoon, J.-H. Lee, H.-W. Lee, J.-W. Son, Physical and electrochemical characteristics of pulsed laser deposited $La_{0.6}Sr_{0.4}CoO_{3-\delta}$-$Ce_{0.9}Gd_{0.1}O_{2-\delta}$ nanocomposites as a function of the mixing ratio, J. Electrochem. Soc. 161 (2014) F16–F22.

[74] C.-A. Thieu, J. Hong, H. Kim, K.J. Yoon, J.-H. Lee, B.-K. Kim, J.-W. Son, Incorporation of a Pd catalyst at the fuel electrode of a thin-film-based solid oxide cell by multi-layer deposition and its impact on low-temperature co-electrolysis. J. Mater. Chem. A 5 (2017) 7433–7444, https://doi.org/10.1039/C7TA00499K.

[75] K. Bae, D.Y. Jang, H.J. Choi, D. Kim, J. Hong, B.-K. Kim, J.-H. Lee, J.-W. Son, J.H. Shim, Demonstrating the potential of yttrium-doped barium zirconate electrolyte for high-performance fuel cells, Nat. Commun. 8 (2017) 14553.

[76] K. Bae, H.-S. Noh, D.Y. Jang, J. Hong, H. Kim, K.J. Yoon, J.-H. Lee, B.-K. Kim, J.H. Shim, J.-W. Son, High-performance thin-film protonic ceramic fuel cells fabricated on anode supports with a non-proton-conducting ceramic matrix, J. Mater. Chem. A 4 (2016) 6395–6403.

[77] H.-Y. Jung, Hierachical control of nano-composite cathode for the performance improvement of intermediate temperature solid oxide fuel cell, Ph.D. Thesis in Dept. Materials Science and Engineering, Seoul National University, Seoul, 2011.